ACS APPLIED MATERIALS & INTERFACES

Research Article

www.acsami.org

Influencing Mechanism of the Selenization Temperature and Time on the Power Conversion Efficiency of $Cu_2ZnSn(S,Se)_4$-Based Solar Cells

Zhen-Yu Xiao,[†,‡] Bin Yao,[*,†,‡] Yong-Feng Li,[*,†,‡] Zhan-Hui Ding,[†,‡] Zhong-Min Gao,[§] Hai-Feng Zhao,[∥] Li-Gong Zhang,[∥] Zhen-Zhong Zhang,[∥] Ying-Rui Sui,[⊥] and Gang Wang[*,#]

[†]Key Laboratory of Physics and Technology for Advanced Batteries (Ministry of Education), College of Physics, Jilin University, Changchun 130012, China

[‡]State Key Lab of Superhard Materials, College of Physics, Jilin University, Changchun 130012, China

[§]State Key Laboratory of Inorganic Synthesis and Preparative Chemistry, College of Chemistry, Jilin University, 2699 Qianjin Street, Changchun 130012, China

[∥]State Key Laboratory of Luminescence and Applications, Changchun Institute of Optics, Fine Mechanics and Physics, Chinese Academy of Sciences, No. 3888 Dongnanhu Road, Changchun 130033, China

[⊥]Key Laboratory of Functional Materials Physics and Chemistry of the Ministry of Education, Jilin Normal University, Siping 136000, China

[#]State Key Laboratory of Rare Earth Resource Utilization, Changchun Institute of Applied Chemistry, Chinese Academy of Sciences, 5625 Renmin Street, Changchun130022, China

ABSTRACT: $Cu_2ZnSn(S,Se)_4$ (CZTSSe) films were deposited on the Mo-coated glass substrates, and the CZTSSe-based solar cells were successfully fabricated by a facile solution method and postselenization technique. The influencing mechanisms of the selenization temperature and time on the power conversion efficiency (PCE), short-circuit current density (J_{sc}), open-circuit voltage (V_{oc}), and fill factor (FF) of the solar cell are systematically investigated by studying the change of the shunt conductance (G_{sh}), series resistance (R_s), diode ideal factor (n), and reversion saturation current density (J_0) with structure and crystal quality of the CZTSSe film and CZTSSe/Mo interface selenized at various temperatures and times. It is found that a $Mo(S_{1-x},Se_x)_2$ (MSSe) layer with hexagonal structure exists at the CZTSSe/Mo interface at the temperature of 500 °C, and its thickness increases with increasing selenization temperature and time. The MSSe has a smaller effect on the R_s, but it has a larger influence on the G_{sh}, n, and J_0. The PCE, V_{oc}, and FF change dominantly with G_{sh}, n, and J_0, while J_{sc} changes with R_s and G_{sh}, but not R_s. These results suggest that the effect of the selenization temperature and time on the PCE is dominantly contributed to the change of the CZTSSe/CdS p−n junction and CZTSSe/MSSe interface induced by variation of the quality of the CZTSSe film and thickness of MSSe in the selenization process. By optimizing the selenization temperature and time, the highest PCE of 7.48% is obtained.

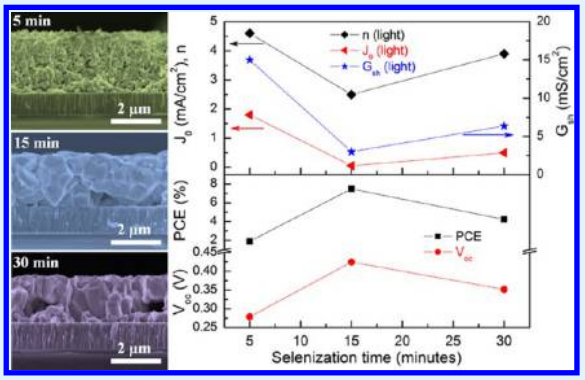

KEYWORDS: *$Cu_2ZnSn(S,Se)_4$, kesterite structure, thin-film solar cell, selenization*

1. INTRODUCTION

Kesterite $Cu_2ZnSn(S,Se)_4$ (CZTSSe) has been identified as a promising absorber material composed of earth-abundant and nontoxic elements, due to not only its optoelectronic properties, such as its high absorption coefficient (>10^4 cm^{-1}) and tunable band gap (1.0−1.5 eV), but also its good photovoltaic performance (a power conversion efficiency (PCE) as much as 33% according to Shockley−Queisser theory).[1−4] Various deposition methods for the fabrication of CZTSSe films have been reported, including coevaporation,[5−7] sputtering,[8−11] electrochemical deposition,[12,13] solution deposition,[14−21] etc. CZTSSe-based solar cells with the highest efficiency (12.7%) have been fabricated by a hydrazine-based solution approach, which is promising as well in the light of the production cost.[21] Among these methods, CZTSSe film is often prepared in a two-step process: first, deposition of a kesterite Cu_2ZnSnS_4 (CZTS) or CZTSSe precursor layer with suitable elemental composition, and subsequently, heat treatment of the precursor in a chalcogen-containing environment. For the latter

Received: May 1, 2016
Accepted: June 21, 2016
Published: June 21, 2016

DOI: 10.1021/acsami.6b05201
ACS Appl. Mater. Interfaces 2016, 8, 17334−17342

step, optimized process control is crucial for obtaining high-performance CZTSSe-based solar cells.

To produce device-quality CZTSSe absorbers with high crystallinity, large grain size, and single kesterite structure, a heat treatment of the precursor films at an elevated temperature (>500 °C) is usually required. However, the CZTSSe films could undergo a significant loss of Sn during annealing temperature above 500 °C.[22−24] The segregation of a binary Zn-chalcogenide secondary phase at the CZTSSe surface is likely related to this Sn loss.[25,26] On the other hand, excessive annealing under a chalcogen-containing atmosphere often results in the formation of a thick $Mo(S_{1-x},Se_x)_2$ (MSSe) layer at the CZTSSe/Mo interface, which may increase the back-contact resistance.[27,28] Therefore, optimization of the annealing temperature and time is crucial for obtaining high quality of CZTSSe films and high PCE CZTSSe-based solar cells.

In recent years, there have been many reports in the literature on the effect of postannealing in a chalcogen-containing environment on structure and crystal quality of the CZTSSe films and PCEs of the CZTSSe-based solar cells.[29−34] However, most of the literature usually focuses on control of structure, e.g., preventing phase segregation, and increment of grain size and compactness of the film as well as effect of them on the properties of the solar cells. Few literature reports are found on the effect of the postannealing on structure and quality of CZTSSe/CdS and CZTSSe/Mo interfaces and the effect of the interfaces on properties of CZTSSe-based solar cells, and the effect of the MSSe on properties of a CZTSSe-based solar cell is still argued up to now.[35−37]

In this work, we prepared CZTSSe films by annealing CZTS precursor films deposited on Mo-coated glass under selenium vapor and systematically investigated the changes of structure and crystal quality of the CZTSSe films and CZTSSe/Mo interfaces. Our work demonstrates that the MSSe layer has a smaller effect on the R_s, but it has a larger influence on the G_{sh}, n, and J_0. The PCE, V_{oc}, and FF change dominantly with G_{sh}, n, and J_0, while J_{sc} changes with R_s and G_{sh} but not R_s. By optimizing the annealing temperature and time, a CZTSSe solar cell with a PCE of 7.48% has been achieved.

2. EXPERIMENTAL DETAILS

A precursor solution used for preparation of CZTS thin films was prepared by dissolving $Cu(CH_3COO)_2{\cdot}H_2O$ (0.7986 g, 4 mmol), $SnCl_2{\cdot}2H_2O$ (0.6205 g, 2.75 mmol), $ZnCl_2$ (0.3816 g, 2.80 mmol), and thiourea (1.005 g, 13.2 mmol) into dimethyl sulfoxide (6 mL, DMSO) and then magnetically stirring for 1 h at room temperature. A detailed synthetic procedure of the precursor solution can be found elsewhere.[20] A CZTS thin film with a thickness of ∼1.5 μm was fabricated by spin-coating the CZTS precursor solution on the molybdenum (Mo)-coated soda lime glass (SLG) substrates at a rotating rate of 3000 rpm for 30 s followed by drying in air at 300 °C, and the coating and drying processes were repeated 10 times. To get the suitable CZTSSe thin films, the as-prepared CZTS films and 100 mg of selenium powder were sealed in a graphite box (∼55 mm in diameter and ∼40 mL in volume), followed by a selenization process in a rapid thermal processing (RTP) furnace (MTI, OTF-1200X-4-RTP) under nitrogen flow (70 mL/min) with a ramping rate of 300 °C/min, and finally cooled down to room temperature naturally. The annealing time is in a period of 5−30 min, and the annealing temperature is in a range of 500−600 °C. CZTSSe-based solar cell devices with traditional structure, i.e., SLG/Mo/CZTSSe/CdS/*i*-ZnO/indium tin oxide (ITO)/Al grid, were prepared by using the CZTSSe films as absorber layers. The CdS buffer layer (∼50 nm) was deposited by chemical bath deposition, and then the *i*-ZnO (∼70 nm) and ITO (∼250 nm) were sputtered on the top of the CdS layer followed by thermal evaporation of the Al grid electrode (∼2 μm) on the top of the ITO layer (the details can be found elsewhere[38]), and finally the whole device was mechanically scribed into 4 small cells with an active area of 0.39 cm^2 for each cell, ∼95% of total device area (0.41 cm^2).

The crystal structures of the films were characterized by an X-ray diffractometer (XRD) with Cu Kα radiation (λ = 1.5406 Å). Raman spectra with an excitation wavelength of 532 nm were recorded using a Renishaw system. The scanning electron microscope (SEM) measurements were performed using a Hitachi S-4800 equipped with an energy-dispersive X-ray spectroscopy (EDS) system (EDAX Genesis 2000). For the power conversion efficiency measurements of CZTSSe-based solar cells, the current density−voltage curves were measured with a Keithley 2400 source meter and a solar simulator (Abet Sun 2000; AM 1.5) by a homemade probe station. The light intensity was calibrated to 100 mW/cm^2 using a Newport optical power meter (model 842-PE) certified by Newport. The external quantum efficiency and reflection curves were measured using a Zolix SCS100 QE system equipped with a 150 W xenon light source, a lock-in amplifier, and an integrating sphere.

3. RESULTS AND DISCUSSION

3.1. Effect of selenization temperature on structure and crystal quality of CZTSSe films and CZTSSe/Mo interfaces. To investigate the effects of annealing temperature on microstructure and crystal quality of the CZTS films during the selenization process, the CZTS films were annealed for 15 min under atmosphere of Se at temperatures of 500, 550, and 600 °C. Figure 1a−d shows the XRD patterns of the as-prepared CZTS film and selenized CZTSSe films. For the as-prepared CZTS film, besides the diffraction peaks of (110) and (211) crystal planes of Mo located at 40.54 and 73.67°, respectively, three diffraction peaks are observed at 28.51, 47.52, and 56.18°, which are closed to the diffraction angles of, respectively, (112), (220), and (312) planes of CZTS with kesterite structure[39−42] and Cu_3SnS_4 with tetragonal structure,[43] and of (111), (220), and (311) planes of Cu_2SnS_3 and ZnS with cubic structure,[44] respectively. So, it is difficult to identify phase compositions of the film only by XRD. To identify the phase compositions, a Raman scattering spectrum was recorded for the CZTS film, as shown in Figure 2a. It is very similar to the Raman spectrum of CZTS with kesterite structure,[40−42] suggesting that the CZTS film consists of a single phase of kesterite CZTS. As shown in Figure 1a, the three diffraction peaks of the as-prepared CZTS film are very weak and broad, indicating that the CZTS film is composed of small-size grains. The average size of the grains is estimated to be 8.0 nm by using Scherrer equation and full width at half-maximum of the (112) peak. After the CZTS film is selenized at temperatures of 500, 550, and 600 °C, more XRD diffraction peaks are observed, as shown in Figure 1b−d. Among the peaks, the diffraction intensities and angles of peaks marked by ◆ are in agreement with those of CZTSSe with kesterite structure, implying that the CZTS film transforms into kesterite CZTSSe film.[39−42] Raman scattering measurement also demonstrates this transformation, as shown in Figure 2b−d, which shows that the intensity of Raman bands of the CZTS decreases sharply after being selenized at 500, 550, and 600 °C; at the same time, four additional Raman bands located at about 175, 200, 237, and 250 cm^{-1} are observed, in agreement with Raman spectrum of kesterite CZTSSe reported in the literature.[40−42] Compared to the CZTS film, XRD diffraction angles of the CZTSSe film shift toward a lower diffraction angle direction, and the angles and full width at half-maximum

DOI: 10.1021/acsami.6b05201
ACS Appl. Mater. Interfaces 2016, 8, 17334−17342

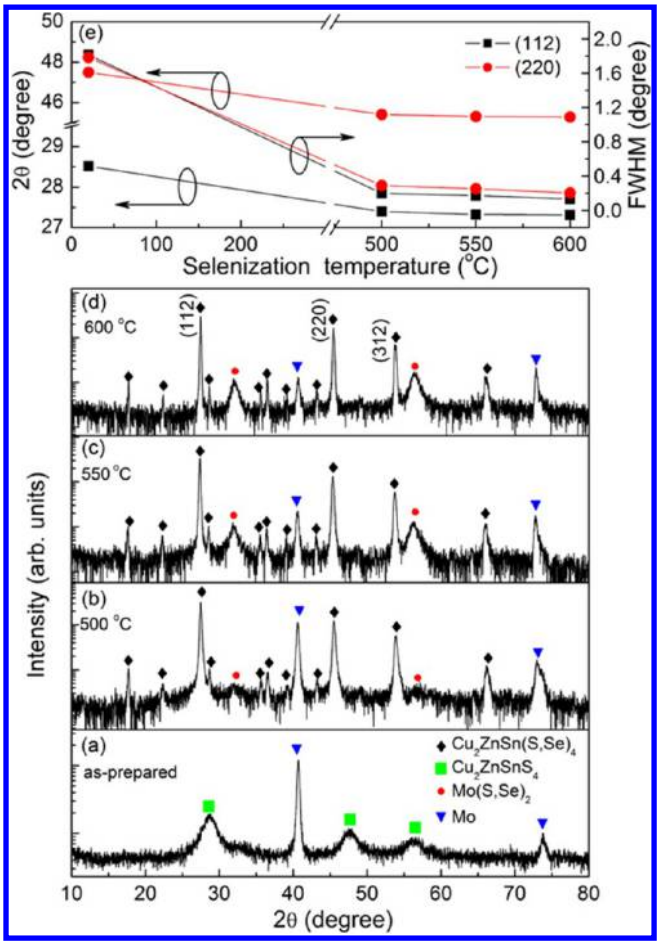

Figure 1. XRD patterns of the CZTS (a) and CZTSSe films obtained at 500 (b), 550 (c), and 600 °C (d). Plots of diffraction intensity and fwhm of (112) and (220) peaks of CZTS and CZTSSe as a function of selenization temperature (e).

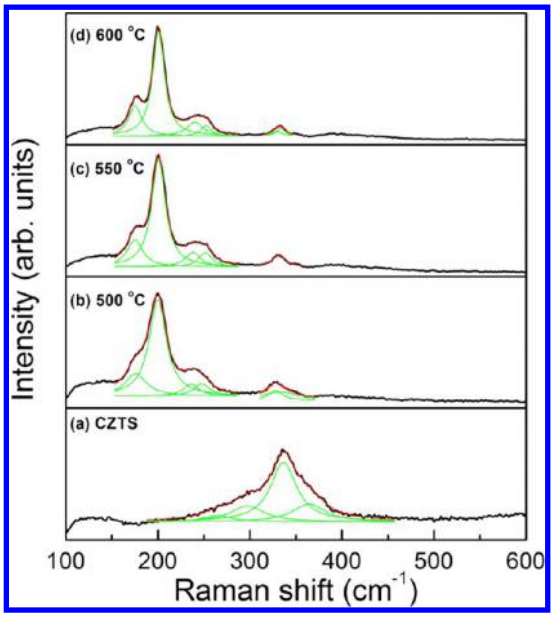

Figure 2. Raman spectra of the CZTS (a) and CZTSSe films obtained at 500 (b), 550 (c), and 600 °C (d).

(fwhm) decrease with increasing selenization temperature, as shown in Figure 1e, demonstrating that the content of Se, the crystal quality, and the grain size of the CZTSSe film increase with improving temperature.

In addition, two additional XRD peaks (marked by ●) are observed near 31.88−31.92° and 56.28−56.49° in Figure 1b−d besides the XRD peaks of the CZTSSe and Mo, which are in the diffraction angle ranges of the (110) and (100) planes of $MoSe_2$ and MoS_2, respectively.[45,46] Moreover, the diffraction angles of both peaks shift to a lower diffraction angle as the selenization temperature increases. The shift is attributed to the increase of Se content in the MSSe with increasing selenization temperature, due to the fact that the ionic radius of Se is larger than that of S. By using Vegard's theorem and lattice constants of the MSSe calculated on the data of Figure 1b−d, the x in the MSSe obtained at selenization temperatures of 500, 550, and 600 °C is calculated to be 0.74, 0.83, and 0.85, respectively, indicating that the MSSe is formed by the reaction of Mo and Se dominantly.

It is also found from Figure 1 that the XRD intensity decreases with increasing the temperature for Mo but increases for the MSSe. Figure 3 shows plots of XRD intensity change of

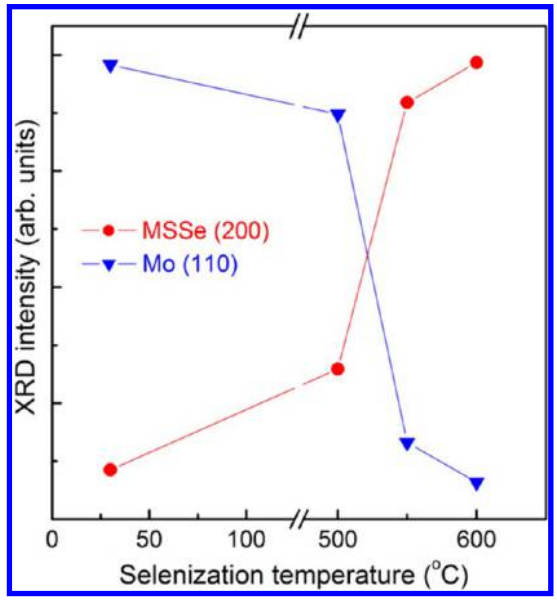

Figure 3. Plots of XRD intensity of the (110) peak of Mo and of the (200) peak of MSSe as a function of the selenization temperature.

the (110) peak of Mo (marked by ▲) and the (200) peak of MSSe (marked by ●) as a function of selenization temperature. Because the areas of all the samples are the same, the XRD intensity change of the MSSe or Mo implies a change of amount (or thickness) of the MSSe or Mo layers. So, Figure 3 indicates that a very small amount of MSSe forms at 500 °C, then the amount of the MSSe increases greatly at temperatures between 500 and 550 °C, and finally the amount increases slowly in the temperature range from 550 to 600 °C. The decrease in the intensity of Mo is due to the fact that the Mo reacts with Se and S to form MSSe, and the higher the temperature, the more the Mo reacts with Se. From the change of the x and of the intensity of MSSe, it is deduced that the MSSe grows quickly between 500 and 550 °C. It is seen in many previous literature reports that the formation of the MSSe layer at the interface of CZTSSe/Mo,[47−50] on one hand, may decrease the series resistance of the solar cell due to the realization of ohmic contact between CZTSSe and Mo; on the

DOI: 10.1021/acsami.6b05201
ACS Appl. Mater. Interfaces 2016, 8, 17334−17342

other hand, it may increase series resistance due to the fact that it is a semiconductor and has higher bulk resistance. Therefore, it is suggested that the MSSe layer should be thinner in order to reduce the series resistance of the solar cell. On the basis of the results of Figures 1 and 3, it seems that 500 °C should be the optimized selenization temperature of the MSSe layer.

However, SEM measurement results for the CZTS and CZTSSe films, as shown in Figure 4, illuminate that the CZTSSe film obtained at 500 °C still consists of nanocrystals, especially at the bottom of the layer. Although the grain sizes increase and the film becomes denser by recrystallization of CZTS during selenization compared to the CZTS film, the grain size of CZTSSe film is still smaller. The small grain size is not favorable to formation of high-efficiency CZTSSe-based solar cells. As the annealing temperature increases to 550 °C, the grains grow sharply to micrometer scale and stack densely, as shown in Figure 4f, but there are many cracks at the film surface, as shown in Figure 4e, which may form traps in the solar cell, leading to recombination of photon-generated carrier and decrease of PCE. Upon further increasing the annealing temperature to 600 °C, although the grain size of the CZTSSe film further increases and the grains stack tightly, there are many big holes in the middle of the film and cracks at the surface, as shown in Figure 4g and h, which will affect improvement of PCE seriously. On the basis of the mentioned results of SEM and XRD, taking account of effects of the grain size of both CZTSSe and MSSe layer on PCE, it is deduced that the optimized selenization temperature should be between 500 and 550 °C for our present work.

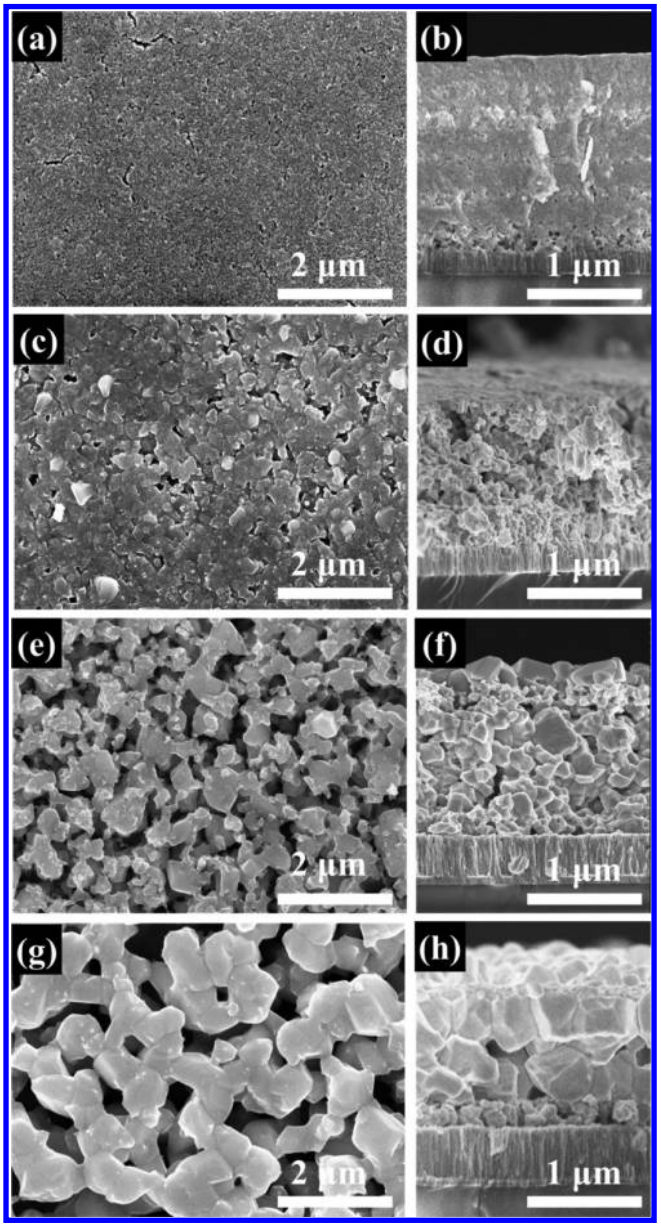

Figure 4. SEM images of surface and cross section of the CZTS (a, b) and CZTSSe thin films obtained at 500 (c, d), 550 (e, d), and 600 °C (g, h).

3.2. Effect of selenization time on structure and crystal quality of CZTSSe films and CZTSSe/Mo interfaces. It is known that the structure and crystal quality of the film is influenced by not only selenization temperature but also selenization time. So we study the effect of selenization time on structure and quality of CZTSSe film and CZTSSe/Mo interface in this section, and the selenization temperature is adopted as 530 °C, which is in the optimized selenization temperature range. Figure 5a–c shows XRD patterns of CZTSSe films obtained by selenization of the CZTS film at 530 °C for 5, 15, and 30 min, respectively. Except for XRD peaks of Mo substrate and MSSe, the XRD peaks marked by ◆ exhibit characteristic reflections of the kesterite CZTSSe phase,[39−42] implying that the CZTSSe films are composed of a single phase of kesterite CZTSSe, which is also confirmed by Raman scattering spectra, as shown in Figure 6. The fwhm decreases sharply in the period of 0−15 min but almost does

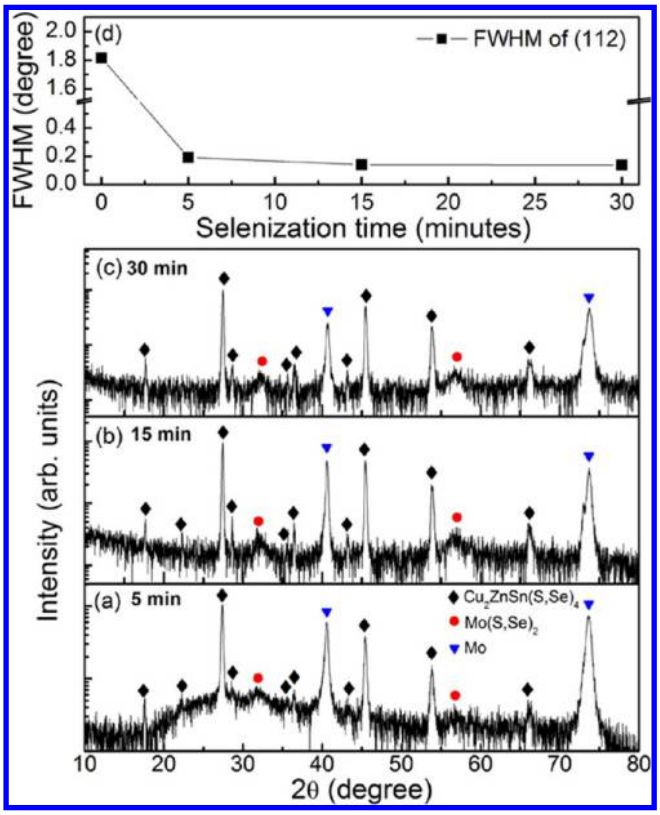

Figure 5. XRD patterns of CZTSSe thin films annealed at 530 °C for 5 (a), 15 (b), and 30 min (c) and plot of fwhm of the (112) peak as a function of selenization time (d).

DOI: 10.1021/acsami.6b05201
ACS Appl. Mater. Interfaces 2016, 8, 17334−17342

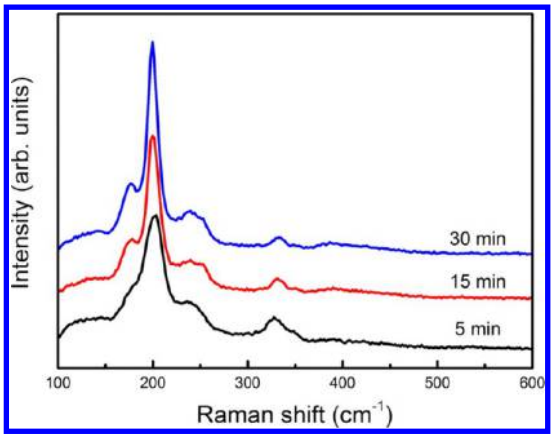

Figure 6. Raman spectra of the CZTSSe films obtained at 5, 15, and 30 min.

not change in the period of 15−30 min, as shown in Figure 5d, indicating that the crystal quality of the CZTSSe film has almost reached the best level at the time of 15 min and changes a little during a period of 15−30 min.

It is also found from Figure 5 that the diffraction intensity decreases with increasing selenization time for Mo but increases for MSSe. Figure 7 plots change of intensity of (110) of Mo

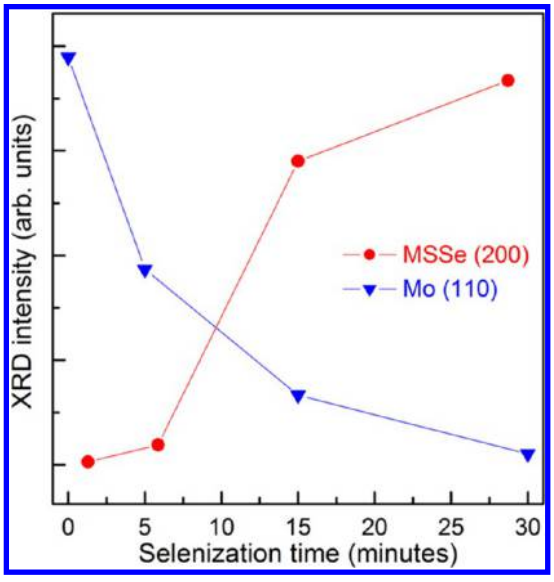

Figure 7. Plots of XRD intensity of (110) peak of Mo and of (200) peak of MSSe as a function of selenization time.

and (200) of MSSe as a function of selenization time, indicating that the diffraction intensity of the MSSe increases slowly in the selenization time of 5 min, then sharply increases in a period of 5−15 min, and slowly changes in a period of 15−30 min. The result of Figure 7 manifests that the thickness of the MSSe layer is very thin as the CZTS is selenized for 5 min, increases sharply upon selenization for 15 min, and increases slowly as selenized in the period of 15−30 min.

The SEM measurements for surface and cross section of the CZTSSe films obtained at the selenization times of 5, 15, and 30 min are shown in Figure 8. It demonstrated that the CZTSSe film obtained at 5 min is composed of nanometer grains, and the grains also stack loosely. Moreover, there are some obvious holes in the CZTSSe film obtained at 5 min, as

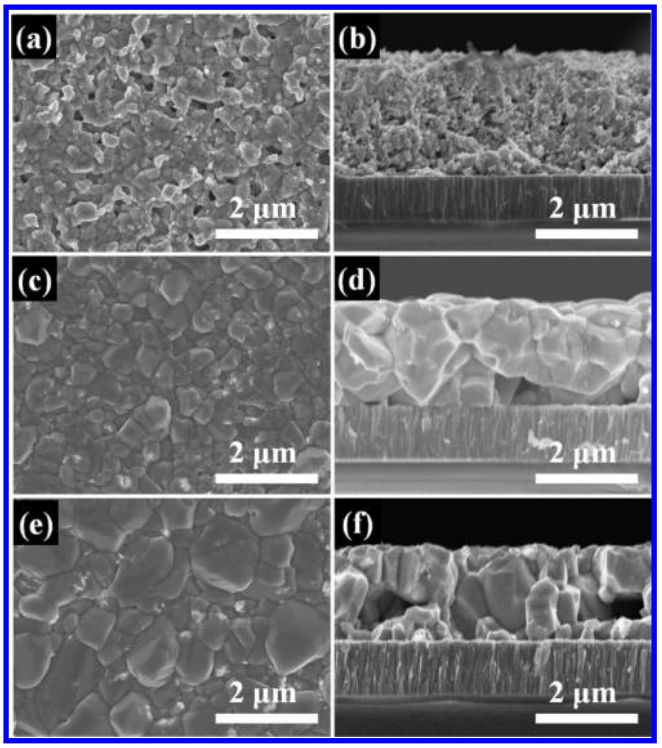

Figure 8. SEM images of surface and cross section of the CZTSSe thin films obtained at 530 °C for 5 (a, b), 15 (c, d), and 30 min (e, f).

shown in Figure 8a and b. However, for the CZTSSe film obtained at 15 min, as shown in Figure 8c and d, the grain increases greatly to be micrometer scale and stacks compactly and the surface is smooth. When the time increases to 30 min, the grain size change little compared to the CZTSSe film obtained at 15 min, as shown in Figure 8e and f. It is known that the CZTSSe film with smooth surface and large grain size is favorable to fabrication of high PCE solar cell. So, the optimized time should be between 5 and 15 min at a selenization temperature of 530 °C, from the point of view of the grain size of the CZTSSe and the thickness of the MSSe in the present work.

3.3. Effect of selenization temperature and time on PCE of solar cells. It is well-known that the PCE is affected mainly by absorber layer, interface of absorber-layer/buffer-layer, and contact of back electrode, which are influenced differently by annealing temperature and time, resulting in the fact that their contributions to the PCE are different. For CZTSSe-based solar cell, it is recognized that the CZTSSe film with large grain size, compact stack, and smooth surface is favorable to preparation of a high PCE solar cell. However, the effect of the MSSe layer formed at the back electrode on the PCE is still argued.[35−37] To understand the mechanism of effect of selenization temperature and time on the PCE, three solar cells with a structure of SLG/Mo/CZTSSe/CdS/i-ZnO/indium tin oxide (ITO)/Al grid were prepared by using the CZTSSe absorber layers prepared at 530 °C in the selenization times of 5, 15, and 30 min and were investigated by measurement of their current density(J)−voltage(V) curves under AM 1.5G illumination. Figure 9 shows the J−V characteristic curves of the three solar cells. The detailed device parameters are listed in Table 1, which indicates that the PCE increases from 1.9% to 7.48% as the time increases from 5 to 15 min, and then decreases to 4.23% as the time increases to

DOI: 10.1021/acsami.6b05201
ACS Appl. Mater. Interfaces 2016, 8, 17334−17342

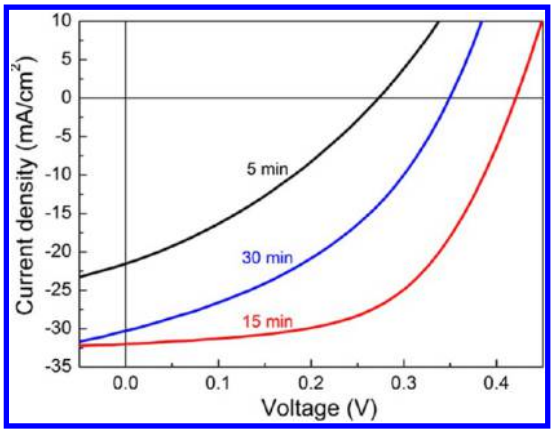

Figure 9. Current−voltage characteristics of the CZTSSe-based solar cell using the CZTSSe absorber layer prepared at a selenization temperature of 530 °C in the periods of 5, 15, and 30 min under AM 1.5G illumination.

30 min. The open-circuit voltage (V_{oc}) and fill factor (FF) change in similar regularity to the PCE, but the short-circuit current density (J_{sc}) does not somewhat: it increases sharply as the time increases from 5 to 15 min and then decreases a little from 15 to 30 min. It is known that PCE = FF × J_{sc} × V_{oc}/P_{in}, where P_{in} is incident power and a constant in PCE measurement. PCE should change directly with FF, J_{sc}, and V_{oc}, and its increase (or decrease) ratio can be expressed as $\Delta PCE/PCE = \Delta FF/FF + \Delta J_{sc}/J_{sc} + \Delta V_{oc}/V_{oc}$. As Table 1 shows, the PCE, J_{sc}, FF, and V_{oc} all increase sharply as the selenization time increases from 5 to 15 min and then decrease from 15 to 30 min. The increase ratio of FF, J_{sc}, and V_{oc} ($\Delta FF/FF$, $\Delta J_{sc}/J_{sc}$, and $\Delta V_{oc}/V_{oc}$) is 74%, 49%, and 52%, respectively, in the time of 5−15 min, but the decrease ratio of FF, J_{sc}, and V_{oc} is 27%, 6%, and 17%, respectively, in the time of 15−30 min. The decrease ratio of the J_{sc} is much less than that of FF and V_{oc}. So, the change of the PCE as a function of selenization time mainly should be due to the contribution of the V_{oc} and FF in the time of 15−30 min.

To understand the origin of the change law of the PCE, the effect of bandgap of the CZTSSe films obtained at 530 °C and selenization times of 5, 15, and 30 min on V_{oc} is investigated first. The bandgaps of the three CZTSSe films are estimated by measuring composition of the CZTSSe films and external quantum efficiency (EQE) of the CZTSSe solar cell.[51−54] Table 2 shows the compositions of the three CZTSSe films measured by EDS, indicating that the Se content decreases with increasing selenization time, while Cu, Sn, and Zn content almost do not change. Because the bandgap of CZTSSe decreases with increasing Se content, it is deduced that the bandgap of the CZTSSe films decreases with increasing

Table 2. Compositions of the CZTSSe Films Prepared at 530 °C and Selenization Times of 5, 15, and 30 min, Respectively

sample	Se (at%)	S (at%)	Sn (at%)	Cu (at%)	Zn (at%)
5 min	47.20	10.34	11.46	17.59	13.42
15 min	50.59	7.12	11.13	17.74	13.42
30 min	51.95	6.25	11.17	17.55	13.08

selenization time, which is confirmed by the EQE shown in Figure 10. It is known that V_{oc} increases with increasing

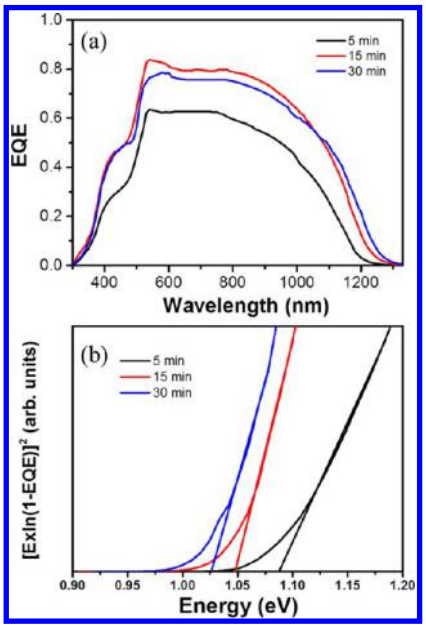

Figure 10. EQE of the CZTSSe-based solar cell using CZTSSe absorber layer prepared at a selenization temperature of 530 °C in the periods of 5, 15, and 30 min (a) and bandgap plots of devices (b).

bandgap when only considering the effect of bandgap on V_{oc};[51−54] as such, it is deduced from the above discussions that the V_{oc} of the CZTSSe-based solar cells should decrease with increasing selenization time, which obviously is different from the change of the V_{oc} shown in Table 1. Therefore, it is deduced that the change of the V_{oc} and its effect on PCE comes from the contribution not of the bandgap of the CZTSSe but of the structure of the solar cell (e.g., p−n junction and back electrode interfaces) and properties of the materials used for preparation of the solar cell (e.g., CZTSSe films, MSSe layer).

It is known that the effect of the structure of the solar cell and the properties of the materials on the PCE of the solar cell is usually characterized by shunt conductance (G_{sh}), series

Table 1. V_{oc}, J_{sc}, FF, and PCE of the CZTSSe-Based Solar Cell Using CZTSSe Absorber Layer Prepared at the Selenization Temperature of 530 °C in the Periods of 5, 15, and 30 min under AM 1.5G Illumination; The Cell Parameters Are the Champion Cell Performances and the Average Values Are Based on 16 Solar Cells (Marked in Italic)

samples	V_{oc} (mV)	J_{sc} (mA/cm²)	FF (%)	eff. (%)
5 min	278.79	21.54	31.75	1.90
	(267.58 ± 11.52)	*(20.16 ± 1.43)*	*(31.27 ± 0.62)*	*(1.68 ± 0.22)*
15 min	424.24	31.98	55.16	7.48
	(412.35 ± 12.04)	*(30.28 ± 1.81)*	*(54.37 ± 2.12)*	*(6.76 ± 0.72)*
30 min	351.52	30.26	39.78	4.23
	(342.66 ± 8.92)	*(28.55 ± 1.77)*	*(35.86 ± 3.92)*	*(3.49 ± 0.74)*

DOI: 10.1021/acsami.6b05201
ACS Appl. Mater. Interfaces 2016, 8, 17334−17342

resistance (R_s), diode ideality factor (n), and reverse saturation current density (J_0) of the solar cell, which can be obtained by analyzing the $J-V$ curves of solar cells with the Sites' method.[55] Table 3 show the G_{sh}, R_s, n, and J_0 of the three solar cells. It can

Table 3. G_{sh}, R_s, n, and J_0 of the CZTSSe-Based Solar Cell Using CZTSSe Absorber Layer Prepared at the Selenization Temperature of 530 °C in the Periods of 5, 15, and 30 min under AM 1.5G Illumination

device	G_{sh} (mS/cm^2)	R_s (Ω cm^2)	n	J_0 (mA/cm^2)
5 min	15.16	1.17	4.63	1.83
15 min	3.12	0.84	2.52	0.05
30 min	6.35	0.52	3.87	0.52

be seen that the R_s decreases monotonously with increasing selenization time. It is known from section 3.2 that the grain size and crystal quality of the CZTSSe as well as the thickness of the MSSe layer increase with increasing selenization time; the former makes the resistivity of the CZTSSe film decrease, as shown in Table 3, resulting in a decrease in R_s, while the latter makes R_s increase. Therefore, it is concluded that the increase in the thickness of the MSSe layer does not make the R_s enlarge but rather decrease, implying that the effect of ohmic contact between the MSSe and Mo on the R_s is much larger than the effect of resistance of the MSSe and that the change of the R_s does not come mainly from the contribution of the MSSe but rather from that of the CZTSSe film. In addition, it is also found that the J_{sc} does not increase monotonously with decreasing R_s, as indicated in many literature reports,[29−34] but rather shows a similar change tendency to R_sG_{sh} with the increasing selenization time, as shown in Figure 11, implying that the J_{sc} is not affected dominantly by the R_s but rather by the G_{sh}.

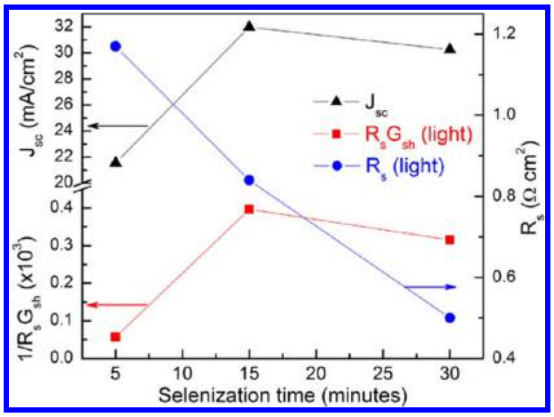

Figure 11. Plots of J_{sc}, R_sG_{sh}, and R_s as a function of selenization time.

It has been mentioned that the change of the PCE is determined by the V_{oc} and FF. On the basis of the results of Tables 1 and 3, we plot the changes of the PCE, V_{oc}, G_{th}, n, and J_0 with the selenizing time, as shown in Figure 12, which illuminates that the change tendency of the V_{oc} and FF with the selenization time is opposite to that of G_{sh} and J_0, in agreement with the relation of V_{oc} and G_{sh} and J_0, which is expressed as

$$V_{oc}G_{sh} = J_{sc}' - J_0(e^{qV_{oc}/nkT} - 1)$$

where q, k, and T are electron charge, Boltzmann constant, and temperature, respectively, and J_{sc}' is short-circuit current

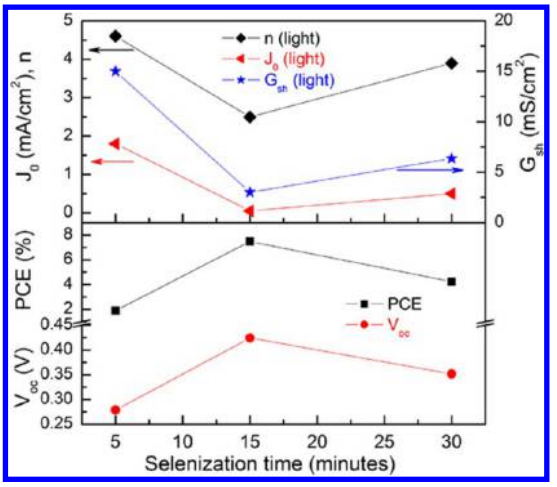

Figure 12. Plots of PCE, V_{oc}, J_0, n, and G_{sh} as a function of selenization time.

density without taking into account R_s and G_{sh}. Because the G_{sh}, n, and J_0 are related to recombination in depletion layers formed at CZTSSe/CdS p−n junction and/or CZTSSe/MSSe, the sharp decrease in G_{sh}, n, and J_0 at the selenization times from 5 to 15 min may be attributed to an increment of quality of the CZTSSe/CdS p−n junction due to the high crystal quality of the CZTSSe film and formation of MSSe, which makes the back electrode be the ohmic contact. However, the slow increase in the G_{sh}, n, and J_0 at times from 15 to 30 min may due to the fact that the thicker MSSe and CZTSSe form a built-in electric field with direction from MSSe to CZTSSe, because it is reported that the MSSe may conduct in n-type.[37,56,57] Moreover, because the MSSe layer is thicker, te photogenerated hole cannot move from CZTSSe to Mo by quantum tunneling effect. So, the built-in field will hinder the move of the photogenerated hole from CZTSSe to Mo electrode and increase recombination of the electron, resulting in an increase of G_{sh}, n, and J_0 and so a decrease in V_{oc}, FF, and PCE.

According to these discussions, it is concluded that the change of the PCE with selenization temperature and time is mainly determined by the change of G_{sh}, n, and J_0, which is related to recombination in CZTSSe/CdS p−n junction and CZTSSe/MSSe interface. The optimized selenization temperature and time are in the range of 500−550 °C and between 5 and 15 min in the present work, respectively.

4. CONCLUSIONS

The effect of selenization temperature and time on the PCE of the CZTSSe-based solar cell is investigated by research on the change of the structure and crystal quality of the CZTSSe film and CZTSSe/Mo interface. It is found that the PCE increases first as the selenization time increases from 5 to 15 min and then decreases with a selenization time of 15−30 min at a selenization temperature of 530 °C. The change is not determined by the R_s but rather by the G_{sh}, n, and J_0. The R_s is mainly affected by the crystal quality of the CZTSSe film, but not the thickness of the MSSe layers, while G_{sh}, n, and J_0 are related to recombination in CZTSSe/CdS p−n junction and CZTSSe/MSSe interface. Therefore, the effect of the selenization temperature and time on the PCE comes dominantly from the contribution of the CZTSSe/CdS p−n junction and the CZTSSe/MSSe interface, induced by the

DOI: 10.1021/acsami.6b05201
ACS Appl. Mater. Interfaces 2016, 8, 17334−17342

variation of CZTSSe crystal quality and the thickness of the MSSe layers. The highest PCE of 7.48% is obtained by optimizing the selenization temperature and time, which are in the range of 500−550 °C and 5−15 min, respectively.

AUTHOR INFORMATION

Corresponding Authors

*E-mail: binyao@jlu.edu.cn.
*E-mail: liyongfeng@jlu.edu.cn.
*E-mail: wsu@ciac.ac.cn.

Notes

The authors declare no competing financial interest.

ACKNOWLEDGMENTS

This work is supported by the National Natural Science Foundation of China under Grant nos. 10874178, 11074093, 61205038, 51302258, 11274135, and 61505067, Specialized Research Fund for the Doctoral Program of Higher Education under Grant no. 20130061130011, Ph.D. Programs Foundation of Ministry of Education of China under Grant no. 20120061120011, and National Found for Fostering Talents of Basic Science under Grant no. J1103202.

REFERENCES

(1) Katagiri, H.; Jimbo, K.; Maw, W. S.; Oishi, K.; Yamazaki, M.; Araki, H.; Takeuchi, A. Development of CZTS-based Thin Film Solar Cells. *Thin Solid Films* **2009**, *517* (7), 2455−2460.

(2) Mitzi, D. B.; Gunawan, O.; Todorov, T. K.; Wang, K.; Guha, S. The Path Towards a High-performance Solution-processed Kesterite Solar Cell. *Sol. Energy Mater. Sol. Cells* **2011**, *95* (6), 1421−1436.

(3) Ki, W.; Hillhouse, H. W. Earth-Abundant Element Photovoltaics Directly from Soluble Precursors with High Yield Using a Non-Toxic Solvent. *Adv. Energy Mater.* **2011**, *1* (5), 732−735.

(4) Ramasamy, K.; Malik, M. A.; O'Brien, P. Routes to Copper Zinc Tin Sulfide Cu_2ZnSnS_4 a Potential Material for Solar Cells. *Chem. Commun.* **2012**, *48* (46), 5703−14.

(5) Shin, B.; Gunawan, O.; Zhu, Y.; Bojarczuk, N. A.; Chey, S. J.; Guha, S. Thin Film Solar Cell with 8.4% Power Conversion Efficiency using an Earth-abundant Cu_2ZnSnS_4 Absorber. *Prog. Photovoltaics* **2013**, *21* (1), 72−76.

(6) Yin, X.; Huang, T. J.; Tang, C.; Du, M.; Sun, L.; Shen, Z.; Gong, H. Significantly Different Mechanical Properties and Interfacial Structures of $Cu_2ZnSn(S,Se)_4$ Films Prepared from Metallic and Sulfur-contained Precursors. *Sol. Energy Mater. Sol. Cells* **2015**, *134*, 389−394.

(7) Lee, Y. S.; Gershon, T.; Gunawan, O.; Todorov, T. K.; Gokmen, T.; Virgus, Y.; Guha, S. $Cu_2ZnSnSe_4$ Thin-Film Solar Cells by Thermal Co-evaporation with 11.6% Efficiency and Improved Minority Carrier Diffusion Length. *Adv. Energy Mater.* **2015**, *5* (7), 1401372.

(8) Dong, Z.-Y.; Li, Y.-F.; Yao, B.; Ding, Z.-H.; Yang, G.; Deng, R.; Fang, X.; Wei, Z.-P.; Liu, L. An Experimental and First-principles Study on Band Alignments at Interfaces of Cu_2ZnSnS_4/CdS/ZnO Heterojunctions. *J. Phys. D: Appl. Phys.* **2014**, *47* (7), 075304.

(9) Yang, G.; Li, Y.-F.; Yao, B.; Ding, Z.-H.; Deng, R.; Qin, J.-M.; Fang, F.; Fang, X.; Wei, Z.-P.; Liu, L. Band Alignments at Interface of Cu_2ZnSnS_4/ZnO Heterojunction: An X-ray Photoelectron Spectroscopy and First-principles Study. *J. Alloys Compd.* **2015**, *628* (0), 293−297.

(10) Scragg, J. J.; Ericson, T.; Fontané, X.; Izquierdo-Roca, V.; Pérez-Rodríguez, A.; Kubart, T.; Edoff, M.; Platzer-Björkman, C. Rapid Annealing of Reactively Sputtered Precursors for Cu_2ZnSnS_4 Solar Cells. *Prog. Photovoltaics* **2014**, *22* (1), 10−17.

(11) Moriya, K.; Tanaka, K.; Uchiki, H. Fabrication of Cu_2ZnSnS_4 Thin-Film Solar Cell Prepared by Pulsed Laser Deposition. *Jpn. J. Appl. Phys.* **2007**, *46* (9A), 5780−5781.

(12) Chen, H.; Ye, Q.; He, X.; Ding, J.; Zhang, Y.; Han, J.; Liu, J.; Liao, C.; Mei, J.; Lau, W. Electrodeposited CZTS Solar Cells from Reline Electrolyte. *Green Chem.* **2014**, *16* (8), 3841.

(13) Jiang, F.; Ikeda, S.; Harada, T.; Ide, A.; Mochihara, A.; Yoshino, K.; Matsumura, M. Fabrication of an Efficient Electrodeposited Cu_2ZnSnS_4-based Solar Cells with More than 6% Conversion Efficiency using a Sprayed Ga-doped ZnO Window Layer. *RSC Adv.* **2014**, *4* (46), 24351.

(14) Wang, G.; Zhao, W.; Cui, Y.; Tian, Q.; Gao, S.; Huang, L.; Pan, D. Fabrication of a $Cu_2ZnSn(S,Se)_4$ Photovoltaic Device by a Low-toxicity Ethanol Solution Process. *ACS Appl. Mater. Interfaces* **2013**, *5* (20), 10042−10047.

(15) Guo, H.; Cui, Y.; Tian, Q.; Gao, S.; Wang, G.; Pan, D. Significantly Enhancing Grain Growth in Cu2ZnSn(S,Se)4 Absorber Layers by Insetting Sb_2S_3, $CuSbS_2$, and $NaSb_5S_8$ Thin Films. *Cryst. Growth Des.* **2015**, *15* (2), 771−777.

(16) Tian, Q.; Cui, Y.; Wang, G.; Pan, D. A Robust and Low-cost Strategy to Prepare Cu_2ZnSnS_4 Precursor Solution and Its Application in $Cu_2ZnSn(S,Se)_4$ Solar Cells. *RSC Adv.* **2015**, *5* (6), 4184−4190.

(17) Xiao, Z.-Y.; Li, Y.-F.; Yao, B.; Deng, R.; Ding, Z.-H.; Wu, T.; Yang, G.; Li, C.-R.; Dong, Z.-Y.; Liu, L.; Zhang, L.-G.; Zhao, H.-F. Bandgap Engineering of $Cu_2Cd_xZn_{1-x}SnS_4$ Alloy for Photovoltaic Applications: A Complementary Experimental and First-principles Study. *J. Appl. Phys.* **2013**, *114* (18), 183506.

(18) Li, C.; Yao, B.; Li, Y.; Xiao, Z.; Ding, Z.; Zhao, H.; Zhang, L.; Zhang, Z. Fabrication, Characterization and Application of $Cu_2ZnSn(S,Se)_4$ Absorber Layer via a Hybrid Ink Containing Ball Milled Powders. *J. Alloys Compd.* **2015**, *643* (0), 152−158.

(19) Xiao, Z.-Y.; Li, Y.-F.; Yao, B.; Ding, Z.-H.; Deng, R.; Zhao, H.-F.; Zhang, L.-G.; Zhang, Z.-Z. Significantly Enhancing the Stability of a Cu_2ZnSnS_4 Aqueous/Ethanol-based Precursor Solution and Its Application In $Cu_2ZnSn(S,Se)_4$ Solar Cells. *RSC Adv.* **2015**, *5* (125), 103451−103457.

(20) Xin, H.; Katahara, J. K.; Braly, I. L.; Hillhouse, H. W. 8% Efficient $Cu_2ZnSn(S,Se)_4$ Solar Cells from Redox Equilibrated Simple Precursors in DMSO. *Adv. Energy Mater.* **2014**, *4* (11), 1301823.

(21) Kim, J.; Hiroi, H.; Todorov, T. K.; Gunawan, O.; Kuwahara, M.; Gokmen, T.; Nair, D.; Hopstaken, M.; Shin, B.; Lee, Y. S.; Wang, W.; Sugimoto, H.; Mitzi, D. B. High Efficiency $Cu_2ZnSn(S,Se)_4$ Solar Cells by Applying a Double In_2S_3/CdS Emitter. *Adv. Mater.* **2014**, *26* (44), 7427−7431.

(22) Weber, A.; Mainz, R.; Schock, H. W. On the Sn Loss from Thin Films of the Material System Cu−Zn−Sn−S in High Vacuum. *J. Appl. Phys.* **2010**, *107* (1), 013516.

(23) Redinger, A.; Berg, D. M.; Dale, P. J.; Siebentritt, S. The Consequences of Kesterite Equilibria for Efficient Solar Cells. *J. Am. Chem. Soc.* **2011**, *133* (10), 3320−3323.

(24) Scragg, J. J.; Ericson, T.; Kubart, T.; Edoff, M.; Platzer-Björkman, C. Chemical Insights into the Instability of Cu_2ZnSnS_4 Films during Annealing. *Chem. Mater.* **2011**, *23* (20), 4625−4633.

(25) Timo Wätjen, J.; Engman, J.; Edoff, M.; Platzer-Björkman, C. Direct Evidence of Current Blocking by ZnSe in $Cu_2ZnSnSe_4$ Solar Cells. *Appl. Phys. Lett.* **2012**, *100* (17), 173510.

(26) Hsu, W.-C.; Repins, I.; Beall, C.; DeHart, C.; Teeter, G.; To, B.; Yang, Y.; Noufi, R. The Effect of Zn Excess on Kesterite Solar Cells. *Sol. Energy Mater. Sol. Cells* **2013**, *113*, 160−164.

(27) Shin, B.; Zhu, Y.; Bojarczuk, N. A.; Jay Chey, S.; Guha, S. Control of an Interfacial $MoSe_2$ Layer in $Cu_2ZnSnSe_4$ Thin Film Solar Cells: 8.9% Power Conversion Efficiency with a TiN Diffusion Barrier. *Appl. Phys. Lett.* **2012**, *101* (5), 053903.

(28) Hsu, C.-J.; Duan, H.-S.; Yang, W.; Zhou, H.; Yang, Y. Benign Solutions and Innovative Sequential Annealing Processes for High Performance $Cu_2ZnSn(Se,S)_4$ Photovoltaics. *Adv. Energy Mater.* **2014**, *4* (6), 1301287.

(29) Chen, G.; Li, J.; Wu, M.; Liu, J.; Lai, F.; Zhu, C. Effect of Post Sulfurization Temperature on the Microstructure of $Cu_2ZnSn(S,Se)_4$ Thin Film. *Mater. Lett.* **2015**, *159*, 32−34.

(30) Gurav, K. V.; Shin, S. W.; Patil, U. M.; Suryawanshi, M. P.; Pawar, S. M.; Gang, M. G.; Vanalakar, S. A.; Yun, J. H.; Kim, J. H.

DOI: 10.1021/acsami.6b05201
ACS Appl. Mater. Interfaces 2016, 8, 17334−17342

Improvement in the Properties of CZTSSe Thin Films by Selenizing Single-step Electrodeposited CZTS Thin Films. *J. Alloys Compd.* **2015**, *631*, 178−182.
(31) Nguyen, D.-C.; Ito, S.; Dung, D. V. A. Effects of Annealing Conditions on Crystallization of the CZTS Absorber and Photovoltaic Properties of $Cu(Zn,Sn)(S,Se)_2$ Solar Cells. *J. Alloys Compd.* **2015**, *632*, 676−680.
(32) Ranjbar, S.; Rajesh Menon, M. R.; Fernandes, P. A.; da Cunha, A. F. Effect of Selenization Conditions on the Growth and Properties of $Cu_2ZnSn(S,Se)_4$ Thin Films. *Thin Solid Films* **2015**, *582*, 188−192.
(33) Hwang, S.; Kim, D.-H.; Son, D.-H.; Yang, K.-J.; Nam, D.; Cheong, H.; Kang, J.-K.; In, S.-i. Effects of a Pre-annealing Treatment (PAT) on $Cu_2ZnSn(S,Se)_4$ Thin Films Prepared by Rapid Thermal Processing (RTP) Selenization. *Sol. Energy Mater. Sol. Cells* **2015**, *143*, 218−225.
(34) Gang, M. G.; Gurav, K. V.; Shin, S. W.; Hong, C. W.; Min, J. H.; Suryawanshi, M. P.; Vanalakar, S. A.; Lee, D. S.; Kim, J. H. A 5.1% Efficient Kesterite Cu_2ZnSnS_4 (CZTS) Thin Film Solar Cell Prepared Using Modified Sulfurization Process. *Phys. Status Solidi C* **2015**, *12* (6), 713−716.
(35) Jarzembowski, E.; Syrowatka, F.; Kaufmann, K.; Fränzel, W.; Hölscher, T.; Scheer, R. The Influence of Sodium on the Molybdenum/$Cu(In,Ga)Se_2$ Interface Recombination Velocity, Determined by Time Resolved Photoluminescence. *Appl. Phys. Lett.* **2015**, *107* (5), 051601.
(36) Scragg, J. J.; Kubart, T.; Wätjen, J. T.; Ericson, T.; Linnarsson, M. K.; Platzer-Björkman, C. Effects of Back Contact Instability on Cu_2ZnSnS_4 Devices and Processes. *Chem. Mater.* **2013**, *25* (15), 3162−3171.
(37) Anand, T. J. S.; Shariza, S. A Study on Molybdenum Sulphoselenide (MoS_xSe_{2-x}, $0 \leq x \leq 2$) Thin Films: Growth from Solution and Its Properties. *Electrochim. Acta* **2012**, *81*, 64−73.
(38) Wang, G.; Wang, S.; Cui, Y.; Pan, D. A Novel and Versatile Strategy to Prepare Metal−Organic Molecular Precursor Solutions and Its Application in $Cu(In,Ga)(S,Se)_2$ Solar Cells. *Chem. Mater.* **2012**, *24* (20), 3993−3997.
(39) Xia, D.; Zheng, Y.; Lei, P.; Zhao, X. Characterization of Cu_2ZnSnS_4 Thin Films Prepared by Solution-based Deposition Techniques. *Phys. Procedia* **2013**, *48* (0), 228−234.
(40) Wang, K.; Gunawan, O.; Todorov, T.; Shin, B.; Chey, S. J.; Bojarczuk, N. A.; Mitzi, D.; Guha, S. Thermally Evaporated Cu_2ZnSnS_4 Solar Cells. *Appl. Phys. Lett.* **2010**, *97* (14), 143508.
(41) Guo, L.; Zhu, Y.; Gunawan, O.; Gokmen, T.; Deline, V. R.; Ahmed, S.; Romankiw, L. T.; Deligianni, H. Electrodeposited $Cu_2ZnSnSe_4$ Thin Film Solar Cell with 7% Power Conversion Efficiency. *Prog. Photovoltaics* **2014**, *22* (1), 58−68.
(42) Wang, K.; Shin, B.; Reuter, K. B.; Todorov, T.; Mitzi, D. B.; Guha, S. Structural and Elemental Characterization of High Efficiency Cu_2ZnSnS_4 Solar Cells. *Appl. Phys. Lett.* **2011**, *98* (5), 051912.
(43) Fernandes, P. A.; Salomé, P. M. P.; Cunha, A. F. d. A Study of Ternary Cu_2SnS_3 and Cu_3SnS_4 Thin Films Prepared by Sulfurizing Stacked Metal Precursors. *J. Phys. D: Appl. Phys.* **2010**, *43* (21), 215403.
(44) Riha, S. C.; Parkinson, B. A.; Prieto, A. L. Solution-Based Synthesis and Characterization of Cu_2ZnSnS_4 Nanocrystals. *J. Am. Chem. Soc.* **2009**, *131* (34), 12054−12055.
(45) James, P.; Lavik, M. The Crystal Structure of $MoSe_2$. *Acta Crystallogr.* **1963**, *16* (11), 1183−1183.
(46) Deng, J.; Yuan, W.; Ren, P.; Wang, Y.; Deng, D.; Zhang, Z.; Bao, X. High-performance hydrogen evolution electrocatalysis by layer-controlled MoS_2 nanosheets. *RSC Adv.* **2014**, *4* (66), 34733−34738.
(47) Jeon, J.-O.; Lee, K. D.; Seul Oh, L.; Seo, S.-W.; Lee, D.-K.; Kim, H.; Jeong, J.-h.; Ko, M. J.; Kim, B.; Son, H. J.; Kim, J. Y. Highly Efficient Copper−Zinc−Tin−Selenide (CZTSe) Solar Cells by Electrodeposition. *ChemSusChem* **2014**, *7* (4), 1073−1077.
(48) Shin, B.; Bojarczuk, N. A.; Guha, S. On the Kinetics of $MoSe_2$ Interfacial Layer Formation in Chalcogen-based Thin Film Solar Cells with a Molybdenum Back Contact. *Appl. Phys. Lett.* **2013**, *102* (9), 091907.
(49) Scragg, J. J.; Wätjen, J. T.; Edoff, M.; Ericson, T.; Kubart, T.; Platzer-Björkman, C. A Detrimental Reaction at the Molybdenum Back Contact in $Cu_2ZnSn(S,Se)_4$ Thin-Film Solar Cells. *J. Am. Chem. Soc.* **2012**, *134* (47), 19330−19333.
(50) Li, J.; Zhang, Y.; Zhao, W.; Nam, D.; Cheong, H.; Wu, L.; Zhou, Z.; Sun, Y. A Temporary Barrier Effect of the Alloy Layer During Selenization: Tailoring the Thickness of $MoSe_2$ for Efficient $Cu_2ZnSnSe_4$ Solar Cells. *Adv. Energy Mater.* **2015**, *5* (9), 1402178.
(51) Zeng, X.; Tai, K. F.; Zhang, T.; Ho, C. W. J.; Chen, X.; Huan, A.; Sum, T. C.; Wong, L. H. $Cu_2ZnSn(S,Se)_4$ Kesterite Solar Cell with 5.1% Efficiency Using Spray Pyrolysis of Aqueous Precursor Solution Followed by Selenization. *Sol. Energy Mater. Sol. Cells* **2014**, *124*, 55−60.
(52) Su, Z.; Tan, J. M. R.; Li, X.; Zeng, X.; Batabyal, S. K.; Wong, L. H. Cation Substitution of Solution-Processed Cu_2ZnSnS_4 Thin Film Solar Cell with over 9% Efficiency. *Adv. Energy Mater.* **2015**, *5* (19), 1500682.
(53) Tai, K. F.; Gunawan, O.; Kuwahara, M.; Chen, S.; Mhaisalkar, S. G.; Huan, C. H. A.; Mitzi, D. B. Fill Factor Losses in $Cu_2ZnSn(S_xSe_{1-x})_4$ Solar Cells: Insights from Physical and Electrical Characterization of Devices and Exfoliated Films. *Adv. Energy Mater.* **2016**, *6* (3), 1501609.
(54) Tai, K. F.; Fu, D.; Chiam, S. Y.; Huan, C. H. A.; Batabyal, S. K.; Wong, L. H. Antimony Doping in Solution-processed $Cu_2ZnSn(S,Se)_4$ Solar Cells. *ChemSusChem* **2015**, *8* (20), 3504−3511.
(55) See http://opvap.com/jsc.php (accessed Jan 27, 2016).
(56) Jin, Y.; Keum, D. H.; An, S.-J.; Kim, J.; Lee, H. S.; Lee, Y. H. A Van Der Waals Homojunction: Ideal p−n Diode Behavior in $MoSe_2$. *Adv. Mater.* **2015**, *27* (37), 5534−5540.
(57) Flöry, N.; Jain, A.; Bharadwaj, P.; Parzefall, M.; Taniguchi, T.; Watanabe, K.; Novotny, L. A $WSe_2/MoSe_2$ Heterostructure Photovoltaic Device. *Appl. Phys. Lett.* **2015**, *107* (12), 123106.

DOI: 10.1021/acsami.6b05201
ACS Appl. Mater. Interfaces 2016, 8, 17334−17342